PCCP

RSC Publishing

PAPER

View Article Online
View Journal | View Issue

Cite this: *Phys. Chem. Chem. Phys.*, 2013, **15**, 9177

Theoretical insights into $[PMo_{12}O_{40}]^{3-}$ grafted on single-walled carbon nanotubes

Shizheng Wen,[ab] Wei Guan,[a] Yuhe Kan,[b] Guochun Yang,[a] Nana Ma,[a] Likai Yan,[a] Zhongmin Su*[a] and Guanhua Chen*[c]

Received 5th March 2013,
Accepted 2nd April 2013

DOI: 10.1039/c3cp51380g

www.rsc.org/pccp

Nano-hybrid materials based on a combination of polyoxometalate (POM) clusters and single-walled carbon nanotubes (SWNT) exhibit a great interesting application in molecular cluster batteries. The interactions between POM and SWNT and their detailed electronic properties have been investigated by employing first-principles calculations. Various models were constructed to study the geometries, interactions (binding sites and energies), and charge transfer behavior. Analysis of charge distributions reveals two different charge transfer characteristic depending on the type of POM interaction with SWNT. The simulation provides insight into the optimal structures in lieu of interfacial stability. Finally, the implications of these results for understanding the properties of molecular cluster batteries are discussed.

1. Introduction

Since the discovery of carbon nanotubes (CNTs), there has been much experimental and theoretical interest in investigating the physical and chemical properties of CNTs.[1–5] The unique structures and properties of CNT make them suitable for a great number of possible applications in multiple research fields.[4,6,7] Chemical functionalization of CNTs offers a magnificent example of processes that utilize the adsorbate to improve the properties of CNTs with specific applications.[4–8] To date, there are two main strategies to modify CNTs, covalent and noncovalent functionalization, which have greatly extended the application of CNTs.[9,10] For the latter approach, noncovalent modification of CNTs can maintain their structural integrity and the electronic properties of both the adsorbate and CNTs to a large extent, and accordingly enhance the overall performance of the complexes, such to improve the solubility of CNTs and the performance of electronic devices.[2] It is also an excellent way to tailor nanosized molecules on a surface for applications in nanoscaled functional electronics.[2]

Polyoxometalates (POMs) have attracted considerable and increasing attention due to their specific chemical and physical properties, which have great potential application in varied fields, such as catalysis,[11,12] medicine,[13] electrochemistry[14] and electronic devices.[15–20] Extensive investigations on modifying the CNTs with POMs have been carried out;[21–38] for example, the $H_3PMo_{12}O_{40}$ was supposed to adsorb on CNTs.[24] Extensive studies also found that the electrochemical properties of POMs could be fully maintained when assembled on CNTs. The nano-hybrid materials greatly enhanced and extended the applications of CNTs.[30–32]

Recently, a new type of lithium battery, the molecular cluster battery (MCB), in which the POM molecules are integrated with single-wall carbon nanotubes (SWNTs), was explored by Yoshikawa and co-workers.[28,29] The hybrid materials were supposed to combine both the unique properties of POMs and SWNTs which were expected to achieve both smooth electron transfer through SWNTs and quick lithium-ion diffusion. The charging–discharging measurements for the hybrid MCBs showed high battery capacity. The special reversible multi-electron redox properties of POMs may explain this extraordinary battery capacity. From transmission electron microscopy (TEM), energy-dispersive X-ray (EDX) spectrum and Mo K-edge XAFS analyses, the POM molecules are separately grafted onto the surfaces of SWNTs without chemical decomposition. The authors speculated that POM ions were electrostatically interacted with the organic cations on the SWNTs.[28,29] However, several works have confirmed that the POMs clusters can graft directly on the CNTs.[24–26] Do the POMs molecules assemble directly on the surface of CNTs and what are the properties of the hybrid materials? Experimental works are limited to elemental analysis of these hybrid materials, so the microscopic geometries and electronic properties of these

[a] *Institute of Functional Material Chemistry, Faculty of Chemistry, Northeast Normal University, Changchun 130024, P. R. China. E-mail: zmsu@nenu.edu.cn; Fax: +86-431-85684009; Tel: +86-431-85099108*
[b] *Jiangsu Province Key Laboratory for Chemistry of Low-Dimensional Materials, School of Chemistry and Chemical Engineering, Huaiyin Normal University, Huaian, 223300, People's Republic of China*
[c] *Department of Chemistry, Centre of Theoretical and Computational Physics, The University of Hong Kong, Hong Kong. E-mail: ghc@everest.hku.hk*

kinds of materials are still unclear. How the POMs affect the electronic structure of CNTs has not yet been reported from a theoretical viewpoint. Therefore, a fundamental theoretical and systematic understanding of POM interaction with SWNT is greatly required. Herein, we present the results of a study on the interaction of POMs and organic molecules with CNTs using periodic density functional calculations.

2. Models and computational details

2.1 Models

As indicated from the experimental results,[28,29] two types of SWNTs, metallic CNT (8,8) and semiconducting CNT (14,0) were chosen with diameters of about 11 Å.[39,40] We consider the supercells with the one-dimensional periodic boundary condition along the tube axis, containing up to 7 unit cells for CNT (8,8) and 4 unit cells for CNT (14,0) with the tube length of 17 Å. The large supercell length was selected because it had been observed in experiment (TEM image) that the molecules were individually adsorbed on the SWNT surface.[28,29] With these dimensions the interactions between the PMo_{12} (PMo_{12} = $[PMo_{12}O_{40}]^{3-}$) molecules and its image were avoided as the distance was long enough. The lateral dimensions (x and y axes) were 30 × 40 Å, which are large enough to prevent the spurious interactions between the images of molecules in these directions. For pristine SWNT investigation, 30 × 30 Å in the x and y axes were chosen instead.

Yoshikawa and co-workers had shown that the battery performances were mainly due to hybridization of the POMs with SWNT, independent of the cations.[29] TBA (TBA = $(C_4H_9)_4N^+$), one of the most common counter cations of Keggin POMs, is selected to keep charge balance in the structural unit.[41] For simplicity, we chose only one TBA to interact with PMo_{12}, and the other two TBA groups are replaced by two Na^+ ions. To minimize the influence of Na affecting the interaction of PMo_{12} and TBA with SWNTs, the positions of the Na are chosen to be far away from the SWNTs as shown in Fig. 2b. The two Na atoms are deposited symmetrically around the PMo_{12} and kept relative unchanged from PMo_{12}. Taking a full account of the molecular symmetry (the PMo_{12} has T_d), the one of favorable ways for the TBA to interact with PMo_{12} may be through S_4 symmetrical axes of PMo_{12} as shown in Fig. 1b. For Keggin $[PW_{12}O_{40}]^{3-}$ interacting with graphene, previous DFT calculation found the S_4 symmetrical axis was more favorable than C_3.[42] So the S_4 symmetrical axis of PMo_{12} was chosen to interact with the CNTs (Fig. 1c). As depicted in Fig. 1c, several initial model geometries have been chosen. For TBA, we have rotated with a step of 45 degrees along the C_2 axis. A few different and randomly chosen starting positions of PMo_{12} along the CNTs surface have also been tried, and they lead to almost the same final result in terms of geometries and energy (mainly accounting for the total and binding energy). In Fig. 2, the eight representative models adopted in the simulations are shown.

2.2 Computational detail

Our DFT calculations are performed using the SIESTA *ab initio* package,[43–45] which employs norm-conserving pseudopotentials

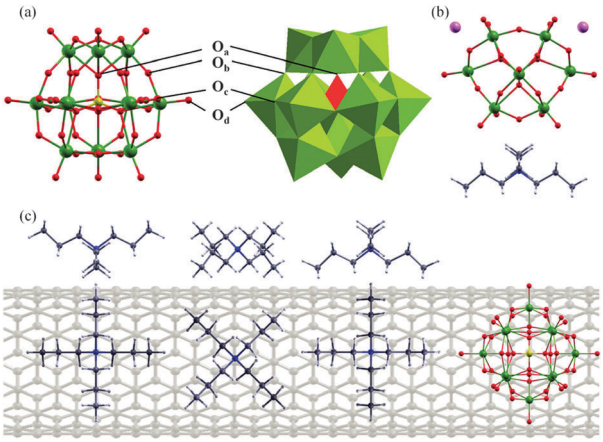

Fig. 1 (a) Ball–stick and polyhedral representations of the Keggin anion $[PMo_{12}O_{40}]^{3-}$. (b) Equilibrium geometry of TBA$[PMo_{12}O_{40}]Na_2$. (c) Scheme of TBA and PMo_{12} assembles on CNTs. Color code: molybdenum (green), oxygen (red), phosphorus (yellow), sodium (pink), carbon (gray), nitrogen (blue) and hydrogen (white).

(Troullier–Martins nonlocal form) and localized atomic orbitals as basis set.[46] A user-defined double-ζ plus polarization (DZP) basis set is constructed for all elements except for Na with an equivalent real-space mesh cutoff of 250 Ry. To describe the Na ion, a basis restricted to only the s orbital and a small cutoff radius (0.497 Bohr) is used in a user defined basis block.[47,48] With this definition, the Na atom has the unit charge $+|e|$ which is defined as a point charge. The geometries are investigated by standard DFT using the local density approximation (LDA) of Ceperley and Alder (CA).[49] The advantage of LDA over the general gradient approximation (GGA) in this work is that the LDA gave us better geometrical results for carbon nanostructures. In addition, the molecular geometries of the POMs are also described well within LDA (see below). Furthermore, the tube–addend interactions are the combination of electrostatic and vdW interactions. For pristine SWNT, we have fully optimized the unit cell structures with a force less than 0.01 eV $Å^{-1}$. The equilibrium C–C bond length is predicted to be 1.422–1.427 Å within LDA, which is in well agreement with the experimental value of 1.42 Å. The band gap for CNT (14,0) is calculated with 0.71 eV under the LDA method. This is consistent with previous works.[40] The detailed pseudopotential reference configurations and cutoff radii for each atom were discussed before.[50]

The van der Waals density functional (vdW-DF) as proposed by Dion *et al.*[51] and recently implemented[52] in the SIESTA code is used to check the energy of the models, as the physisorption of POMs on the CNTs is supposed. For some of the models, we also used the GGA of Perdew, Burke and Ernzerhof (PBE)[53] to explore the geometry and energy properties (Table 2).

All the models are fully optimized without any symmetry constrained by conjugate gradients until the total residual interatomic forces are smaller than 0.02 eV $Å^{-1}$. Due to the large supercell size and atomic number involved (224 carbons in CNT and 96 atoms in TBA–PMo_{12} fragment), the Brillouin zone sampling was performed with 6 K-points along the z axes. Single point calculations with larger K-points (a sampling of 1 × 1 × 100 Monkhorst–Pack grids) were

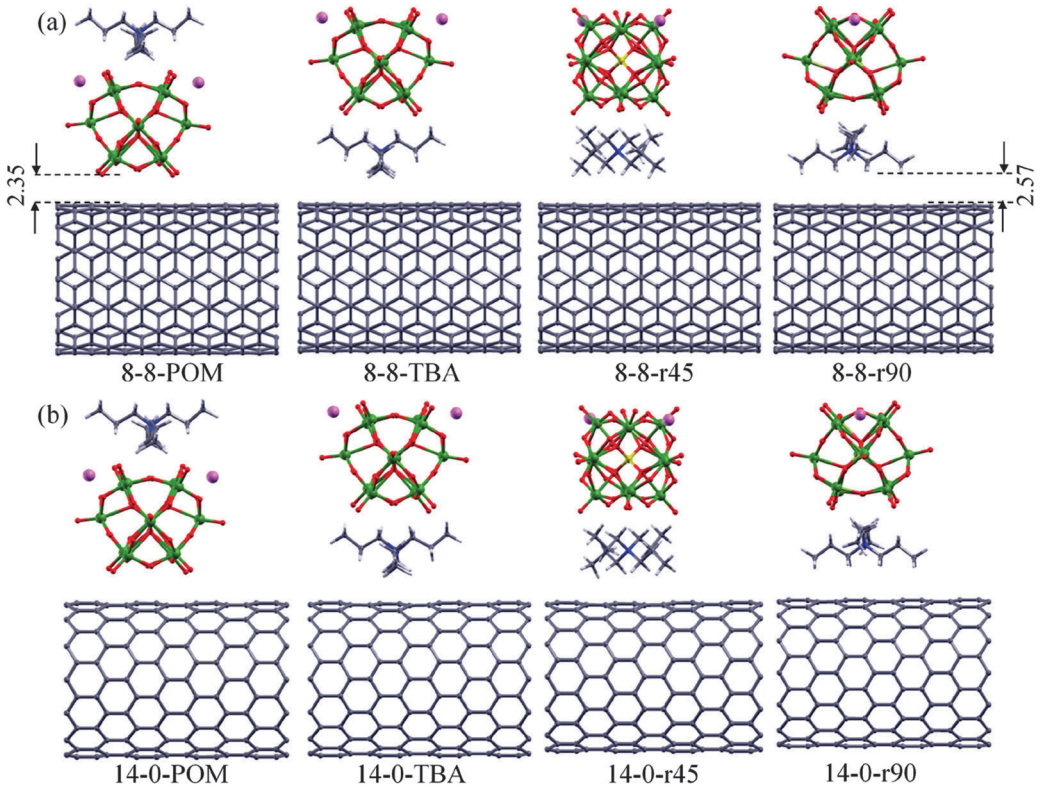

Fig. 2 The equilibrium geometries of TBA–PMo_{12} attached to CNTs. (a) Metallic CNT (8,8), (b) semiconducting CNT (14,0). The labels of the models are defined according to their direct attraction to the CNT surface. Here, the 'r45' and 'r90' represent the degree rotated along the main C_2 symmetrical axes of TBA relative to '-TBA' models.

then performed to obtain the density of states and band structures based on the optimized structures. The charge analysis is based on Mulliken population methods.[54] Figures were generated using the XCrySDen program.[55]

3. Results and discussion

3.1 The properties of PMo_{12}

The geometry and electronic properties of several POM molecules have been explored before using the SIESTA code.[42,48,50] The methodology in the SIESTA code has been checked to reproduce well the geometry of the POM molecules. The main geometric parameters of PMo_{12} calculated by the SIESTA code are summarized in Table 1. Four types of oxygen in PMo_{12}, as depicted in Fig. 1a, are used to illustrate the geometrical character. As shown in the Table, the optimized LDA bond-lengths well-reproduced the experimental data, while the GGA gives increased bond lengths. The results are in good agreement with previous DFT calculations for the same molecule.[56–58] As discussed before, due to the high oxidation state of Mo in PMo_{12}, the t_{2g}-like orbitals are the primary interest for POMs; in addition the electrochemical properties are mainly dominated by these orbitals (LUMOs).[58] The influence and properties of these orbitals caused by the CNTs are discussed below.

Table 1 Selected main bond length for isolated anion PMo_{12} (in unit of Å)

	LDA	GGA	Exp.
P–O	1.56	1.58	1.54
Mo–O_a	2.41	2.46	2.44
Mo–O_b	1.89	1.93	1.91
Mo–O_c	1.91	1.94	1.92
Mo–O_d	1.67	1.70	1.68

3.2 Adsorption configurations and adsorption energy

Molecular dynamics could be one of the effective methods to pre-select molecular geometries of interface models.[39,59–61] However, it is limited in revealing electronic properties and in describing the character of charge transfer. So, we instead employed first-principles calculations to explore the electronic character. Here, taking full account of the structural character, we chose a few different starting positions of the adsorbates to assemble on the CNTs' surface (Fig. 1c). Fig. 2 shows results for the equilibrium geometries of POMs assembled on the CNTs. We have divided them into two groups based upon the type of CNT: metallic CNT (8,8) (Fig. 2a) and semiconducting CNT (14,0) (Fig. 2b). In each group, two situations are discussed. One is the PMo_{12} fragment of the molecule directly interacting with the CNTs and the other one is the PMo_{12} interacting through the TBA mediator. For the latter, due to a different interaction area with CNTs, two more configurations are discussed, denoted by the rotation degree along the main C_2 axes.

To obtain the rough distance between the molecule and CNTs, the vertical distance d is calculated as the average z coordinate of atoms in the interface (closest to each other). The

Table 2 The vertical distance of TBA–PMo_{12} above the CNT surface (d), the adsorption energy (E_{ad}), and the Mulliken charge distribution with the LDA method

	d		E_{ad}/eV			Charge ($\|e\|$)		
Model	LDA	GGA	LDA[a]	GGA[a]	vdW[b]	POM@2Na	TBA	CNT
14-0-POM	2.35	2.60	−1.10(−0.68)	−0.45(−0.15)	−1.41	−1.29	0.80	0.49
14-0-TBA	2.38	2.62	−0.60(−0.38)	−0.30(−0.06)	−0.97	−0.86	0.65	0.22
14-0-r45	2.37	—	−0.64(−0.40)	—	—	−0.87	0.68	0.21
14-0-r90	2.57	—	−0.55(−0.36)	—	—	−0.85	0.67	0.18
8-8-POM	2.34	2.59	−0.98(−0.56)	−0.36(−0.08)	−1.22	−1.18	0.81	0.38
8-8-TBA	2.36	2.63	−0.61(−0.38)	−0.22(−0.06)	−0.82	−0.87	0.68	0.19
8-8-r45	2.43	—	−0.60(−0.38)	—	—	−0.87	0.66	0.21
8-8-r90	2.61	—	−0.51(−0.32)	—	—	−0.85	0.70	0.15
TBA–POM	—	—	—	—	—	−0.91	0.91	—

[a] The binding energies with BSSE correction are shown in brackets. [b] The geometries are based on the results under LDA optimization.

overall distance between the molecule and the CNTs surface is about 2.4 Å, which is similar to the results of $[PW_{12}O_{40}]^{3-}$ adsorbed on graphene.[42] These distances are within the sum range of van der Waals radii of related interfacial atoms. Total charge density plotting (not shown) indicated that no chemical bonding between the molecule and CNTs is formed, which also confirm a van-der-Waals-type interaction. As shown in Table 2, the perpendicular distances of 8-8-POM and 14-0-POM are smaller than other cases, which is in conformity with the adsorption energy calculation below. With the respective rotation of TBA, a slightly different vertical distance showed. Especially for 'r90' cases, about 0.2 Å larger distances were obtained for both metallic and semiconductor CNTs than others.

Four models (8-8-POM, 8-8-TBA, 14-0-POM, and 14-0-TBA) are also fully optimized with the GGA–PBE level. The vertical distances are larger than the LDA results, as shown in Table 2. Similar trends are expected for the GGA method with the LDA. The same trend of the LDA and GGA confirms the optimization results of electronic structures for POM adsorption on the CNTs.

The noncovalent interaction induces slightly geometrical changes for POM and CNTs in all models. We define the distortion energy as: $E_d = E_{tot.}(\text{distorted}) - E_{tot.}(\text{ideal})$, to check the change in the structures.[62] The total energies of 'distorted' and 'ideal' mean the energies of molecules interacting with other and fully relaxed alone, respectively. No greater than 0.1 eV distortion energies were found for both the CNTs and PMo_{12}. For example, for 8-8-POM, the distortion energy of CNT is about 0.012 eV and 0.062 eV for the POM part. These confirm the relative stable properties of CNT and POMs.

To investigate the affinity between the TBA–PMo_{12} and CNT, the adsorption energy was obtained from the following definition:

$$E_{ad} = E_{tot.}(\text{POM + CNT}) - E_{tot.}(\text{POM}) - E_{tot.}(\text{CNT})$$

where $E_{tot.}$ is the total energy of the system, and $E_{tot.}$(POM) includes the TBA part. The basis set superposition error (BSSE) is taken into consideration for corrections (as shown in Table 2, the energies in brackets in the E_{ad} column consider the BSSE corrections). In the definition of E_{ad} we adopted, the more-negative values denote a more-favourable interaction of the complex. As shown in Table 2, all the calculated E_{ad} are negative, which mean the adsorption is energetically favourable. Furthermore, from the viewpoint of energy, the PMo_{12} is more favourable to directly graft onto the CNTs than through the mediator of TBA. Even for the physisorption type, the BSSE has a large effect on the E_{ad}. Also, similar vertical distances are shown for each corresponding model in both groups. For the cases of 14-0-POM and 8-8-POM, the semiconducting CNT(14,0) is energetically preferred over the metallic CNT(8,8) by 0.12 eV. However, for other cases (CNT–TBA) an almost identical E_{ad} was calculated, as listed in Table 2. The DFT–LDA and DFT–GGA methods are known to fail for cases where the adsorption is dominated by van der Waals forces.[51] In Table 2, we also list the calculated E_{ad} with the vdW-DF method. The geometries were based on the LDA optimization results. No further optimization has been performed with vdW-DF due to the inefficient implementation of this method. From Table 2, the calculated results are in accordance with the LDA results without BSSE, which indicates an appropriate description of the system with LDA. The favourable binding interaction is in accordance with the experimental observations on these systems.[28,29] From the simulation results, the favourable configurations are from the direct interactions between POMs and the CNTs rather than the indirect interactions through the organic mediator, from an energy viewpoint. The semiconducting CNT(14,0) has stronger binding interaction with POMs than metallic CNT(8,8).

3.3 Charge transfer characteristic

Another important aspect of these complexes is the charge transfer behaviour. The Mulliken population method was adopted to analyze the charge distribution. As summarized in Table 2, the CNTs act as a charge donor in all models. According to the different configurations, two types of charge transfer results are mainly shown (Fig. 3c and d). For both groups, the 8-8-POM and 14-0-POM transfer a much larger amount of charge from the CNTs to the molecules than others. This may be due to the strong acceptor characteristic of POMs. From the calculated results, it is also found that the TBA in these two models accepted 0.1 e (defined as Type-I, Fig. 3c), while for other models, the POMs' charge distribution remains almost unchanged compared to the sole molecule (TBA-PMo_{12}, in the last row). We define this kind of charge transfer as Type-II (Fig. 3d).

Further insight can be gained from charge density difference (CDD) plotting.[42] In Fig. 3a and b, we plot the CDD which is defined as:

$$\rho_{diff}(\vec{r}) = \rho_{POM\text{-}CNT}(\vec{r}) - \rho_{POM}(\vec{r}) - \rho_{CNT}(\vec{r})$$

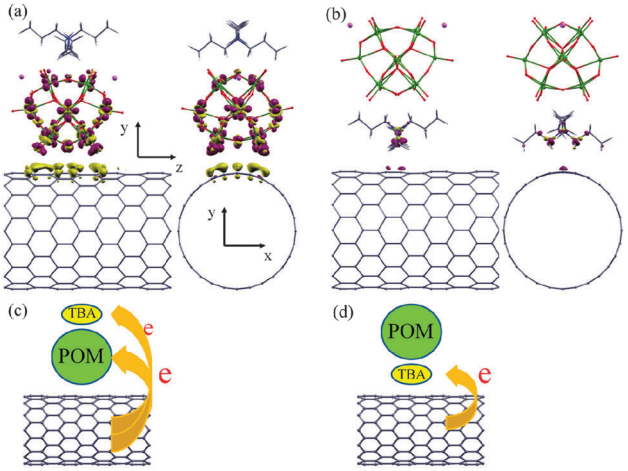

Fig. 3 Plot of charge density difference for (a) 14-0-POM and (b) 14-0-TBA models. The isovalue is set to be ±0.001 e (a.u.)$^{-3}$ in XCrySDen. The violet color represents charge density increasing, while the yellow color means decreasing. (c and d) Schemes of two types of charge transfer.

where $\rho_{\text{POM-CNT}}(\vec{r})$, $\rho_{\text{POM}}(\vec{r})$, and $\rho_{\text{CNT}}(\vec{r})$ are the charge densities of the POM–CNT complex, isolated molecule TBA–POM and pure CNTs, respectively. This partitioning of charge density in real space is useful to define the interaction and the charge transfer between the two subsystems. Here, it should be noted that the charge density refers to the valence electron of atoms as the pseudopotential method we employed in our calculations. From the above definition, the CDD plotting could clearly show the change of charge distribution. In Fig. 3a and b, the violet colour represents the area where charge density increases, while the yellow colour means an area where it decreases. The 3D CDD plotting shows that the increasing charge densities in PMo_{12} mainly reside among the Mo 4d orbital (Fig. 3a). In Fig. 3b, the N and adjacent C have greater increase in charge density. We defined these two different charge transfers as Type-I and Type-II, as shown in Fig. 3c and d. The difference between these two types of charge transfer phenomena may mainly be attributed to the different binding strength of the systems. For PMo_{12} molecule, which directly integrated over the surface of CNTs, a greater amount of charge transfer would be expected. These charge transfer characteristics are different from the previous result of POMs@graphene.[42] This specific charge transfer may be helpful in improving the performance of CNT in electronic device application.

3.4 Electronic properties

To further examine the effect of electronic properties of the TBA–PMo_{12} adsorption on CNTs, the electronic band structures of CNT(8,8) and CNT(14,0) near the Fermi level with the projected density of state (PDOS) approach have been calculated and presented in Fig. 4 and 5. For convenience, in each group we

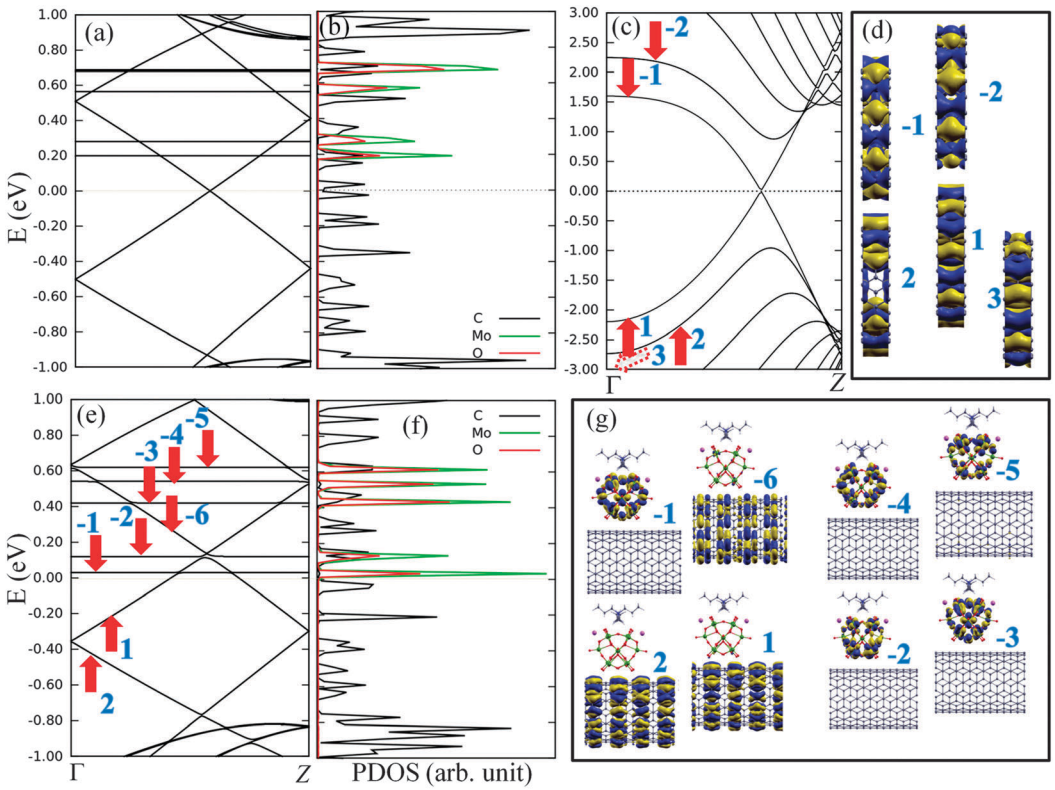

Fig. 4 The calculated band structures and the corresponding PDOS of the molecules grafted on CNT(8,8). (a and b) Band structure and PDOS for 8-8-TBA, (e and f) band structure and PDOS for 8-8-POM, (c) band structure for a pure unit cell of CNT(8,8), (d) and (g) the corresponding isosurface charge densities of states at the Γ-point, labelled as red arrows and Arabic numerals in the band structures. The isosurface value is ±0.05 eV Å^{-1}. For PDOS, three types of atoms are displayed, where 'Mo' and 'O' means the sum of all molybdenum and oxygen atoms in PMo_{12}, and 'C' means the carbon atoms from the CNTs.

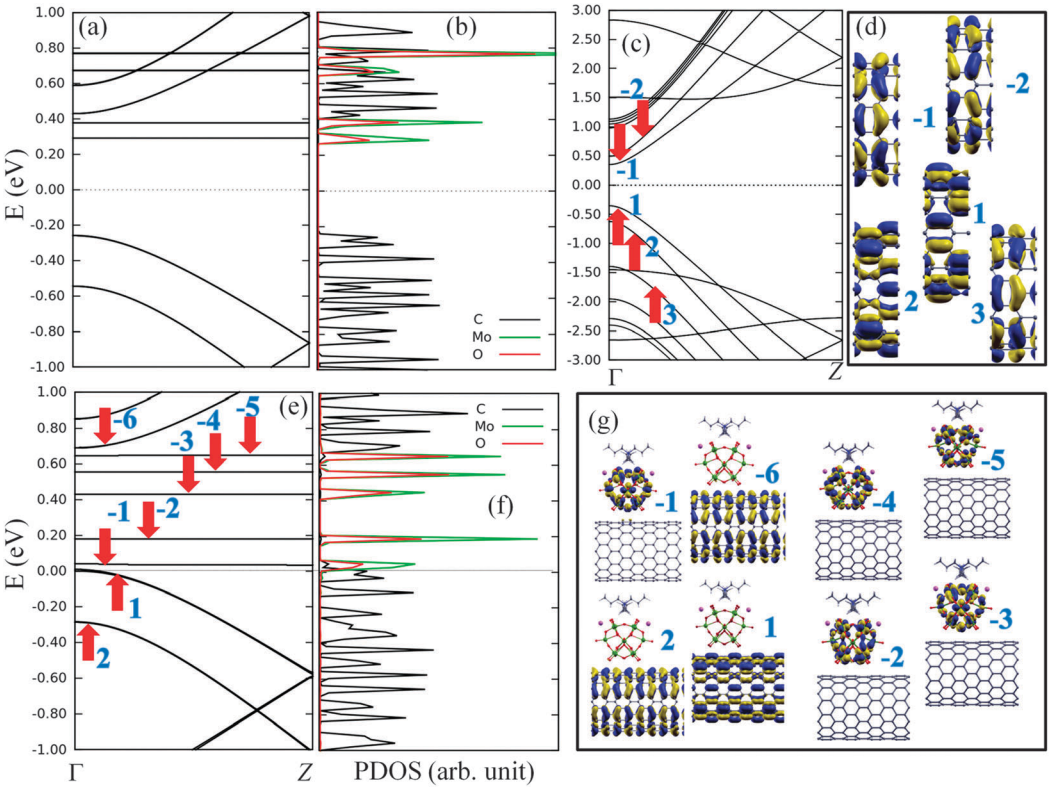

Fig. 5 Calculated band structures and the corresponding PDOS of the molecules grafted on CNT (14,0). (a and b) Band structure and PDOS for 14-0-TBA, (e and f) band structure and PDOS for 14-0-POM, (c) band structure for pure unit cell of CNT (14,0), (d) and (g) the corresponding isosurface charge densities of states at the Γ-point labelled as red arrows and Arabic numerals in the band structures. The isosurface value is ± 0.05 eV Å^{-1}. For PDOS, three types of atoms are displayed. 'Mo' and 'O' mean the sum of all molybdenum and oxygen atoms in PMo_{12}, and 'C' means the carbon atoms from the CNTs.

only show the first two models, as the other two models left similar properties and exhibited only slight differences.

In Fig. 4, we calculated the band structures and PDOS for one of the two models of PMo_{12} grafted on the CNT(8,8). The corresponding charge densities of states at the Γ-point are depicted for checking. Specifically, we label several band states with Arabic numerals in the Figure to denote the relative states with plotting of unit cell CNTs in Fig. 4d. After the POMs adsorption, the metallic character of the CNT(8,8) is retained and the overall electronic structures was not affected strongly for all models. The flat bands in Fig. 4a and e are mainly attributed to the PMo_{12} (with help of PDOS analysis in Fig. 4b and f). For the 8-8-POM model, the CNT(8,8) subbands at the crossing points has been significant perturbed and the Fermi level of CNT has shifted downward by about 0.13 eV. This may be due to stronger binding interaction and the obvious charge transfer from the CNT to PMo_{12}. The flat bands had increased the DOS of the conduction bands, which should improve the conducting properties of the systems. For the 8-8-TBA case, the Fermi level remains unchanged after interaction with TBA–PMo_{12} as the crossing point aligns with the Fermi level of the system. Compared to the 8-8-POM case, the flat bands are slightly further away from the Fermi level, which may be due to the weaker interaction between TBA–PMo_{12} and CNT. It is worth mentioning that we have found, with different types of interfaces (TBA–CNT and PMo_{12}–CNT), a distinct perturbing effect on the electronic properties of CNT. Also, as discussed above, these different styles of interactions correspond to two types of charge transfer.

For semiconducting nanotubes, the adsorption of TBA–PMo_{12} has a significant effect on the electronic properties of CNT (Fig. 5a and e). For the 14-0-TBA case, the band-gap was reduced from 0.71 to 0.53 eV. Here we observe nearly-metallic behaviour for the 14-0-POM case, which is mainly due to the significant effect of PMo_{12} on the valence band of CNT and the empty Mo 4d orbitals appearing above the Fermi level. The strong binding interaction results in an upward shift of the valence band near to the Fermi level. It is worth mentioning that the valence band minimum of 14-0-POM ('**1**' in Fig. 5e) has dual degeneracy, which is composed of the '**1**' and '**2**' band of CNT(14,0) shown in Fig. 5d. Another important characteristic which is similar to the 8-8-POM case is the flat bands just above the Fermi level. They mainly come from the PMo_{12} as indicated by the PDOS analysis (Fig. 5f). These two factors tailor significantly the band gap of CNT(14,0), which changes to nearly-conducting. According to these results, we conclude that a semiconducting CNT changes its electronic properties after the PMo_{12} adsorption. The nearly metallic properties of the SWNTs would promote charge transfer in the molecular cluster batteries. As investigated in experiment, introducing the Keggin PMo_{12} had significantly improved the performance of batteries which may be due to the strong interaction between the PMo_{12}

and CNT. Our results indicate that the POMs molecules with CNT would significantly affect the properties of semiconducting nanotubes. This should also be helpful to understand the structural and electronic properties of these kinds of systems.

4. Conclusions

In summary, the electronic band structures of functionalized SWNTs by the Keggin PMo_{12} anion and the TBA–PMo_{12}–CNT interactions have been revealed by DFT computations with periodic boundary conditions for the first time. Two different interfacial interactions were explored. The semiconductor nanotubes bind TBA–PMo_{12} strongly, and hence are more reactive than their metallic counterparts. Also, from binding energy analysis, the PMo_{12} prefer to bind directly with CNT rather than through the organic mediator. The TBA–PMo_{12} additions are confirmed to result in a change from semiconducting to nearly metallic properties in CNT(14,0). Two different charge transfer characteristics are shown for these systems. Due to the acceptor properties of PMo_{12}, the charge transfers from CNT to PMo_{12} or from CNT to TBA. Such charge transfer and band engineering would be helpful to understand the experimental results of their application in molecular cluster batteries. Thus, such dependence of the electronic properties on the degree of functionalization of SWNTs suggests a novel method for enriching application of carbon nanotubes in electronic devices.

Acknowledgements

The authors gratefully acknowledge financial support from NSFC (21073030 and 21131001) and Doctoral Fund of Ministry of Education of China (20100043120007).

Notes and references

1 R. H. Baughman, A. A. Zakhidov and W. A. de Heer, Carbon nanotubes – the route toward applications, *Science*, 2002, **297**, 787–792.
2 D. A. Britz and A. N. Khlobystov, Noncovalent interactions of molecules with single walled carbon nanotubes, *Chem. Soc. Rev.*, 2006, **35**, 637–659.
3 D. Eder, Carbon nanotube–inorganic hybrids, *Chem. Rev.*, 2010, **110**, 1348–1385.
4 N. Karousis, N. Tagmatarchis and D. Tasis, Current progress on the chemical modification of carbon nanotubes, *Chem. Rev.*, 2010, **110**, 5366–5397.
5 R. Zhou, R. Liu, L. Li, X. Wu and X. C. Zeng, Carbon nanotube superarchitectures: an *ab initio* study, *J. Phys. Chem. C*, 2011, **115**, 18174–18185.
6 J. Liu and M. C. Hersam, in Carbon nanotube sorting and selective growth, *MRS Bull.*, 2010, **35**, 315–321.
7 W. Zhou, S. Zhan, L. Ding and J. Liu, General rules for selective growth of enriched semiconducting single walled carbon nanotubes with water vapor as *in situ* etchant, *J. Am. Chem. Soc.*, 2012, **134**, 14019–14026.
8 J. Wu, K. Gerstandt, H. Zhang, J. Liu and B. J. Hinds, Electrophoretically induced aqueous flow through single-walled carbon nanotube membranes, *Nat. Nanotechnol.*, 2012, **7**, 133–139.
9 Y. L. Zhao and J. F. Stoddart, Noncovalent functionalization of single-walled carbon nanotubes, *Acc. Chem. Res.*, 2009, **42**, 1161–1171.
10 H. Li and J. J. Cooper-White, Hyperbranched polymer mediated fabrication of water soluble carbon nanotube–metal nanoparticle hybrids, *Nanoscale*, 2013, **5**, 2915–2920.
11 N. Mizuno and M. Misono, Heterogeneous catalysis, *Chem. Rev.*, 1998, **98**, 199–217.
12 H. Lv, Y. V. Geletii, C. Zhao, J. W. Vickers, G. Zhu, Z. Luo, J. Song, T. Lian, D. G. Musaev and C. L. Hill, Polyoxometalate water oxidation catalysts and the production of green fuel, *Chem. Soc. Rev.*, 2012, **41**, 7572–7589.
13 J. T. Rhule, C. L. Hill, D. A. Judd and R. F. Schinazi, Polyoxometalates in medicine, *Chem. Rev.*, 1998, **98**, 327–358.
14 M. Sadakane and E. Steckhan, Electrochemical properties of polyoxometalates as electrocatalysts., *Chem. Rev.*, 1998, **98**, 219–238.
15 C. M. Granadeiro, S. Cruz, G. A. B. Gonçalves, P. Marques, P. M. F. J. Costa, R. Ferreira, L. A. D. Carlos and H. Nogueira, Photoluminescent bimetallic-3-hydroxypicolinate/graphene oxide nanocomposite, *RSC Adv.*, 2012, **2**, 9443–9447.
16 J. Lehmann, A. Gaita-Ariño, E. Coronado and D. Loss, Spin qubits with electrically gated polyoxometalate molecules, *Nat. Nanotechnol.*, 2007, **2**, 312–317.
17 A. M. Douvas, E. Makarona, N. Glezos, P. Argitis, J. A. Mielczarski and E. Mielczarski, Polyoxometalate-based layered structures for charge transport control in molecular devices, *ACS Nano*, 2008, **2**, 733–742.
18 E. Kapetanakis, A. M. Douvas, D. Velessiotis, E. Makarona, P. Argitis, N. Glezos and P. Normand, Molecular storage elements for proton memory devices, *Adv. Mater.*, 2008, **20**, 4568–4574.
19 J. M. Clemente-Juan, E. Coronado and A. Gaita-Ariño, Magnetic polyoxometalates: from molecular magnetism to molecular spintronics and quantum computing, *Chem. Soc. Rev.*, 2012, **41**, 7464–7478.
20 H. Wang, S. Hamanaka, Y. Nishimoto, S. Irle, T. Yokoyama, H. Yoshikawa and K. Awaga, In operando X-ray absorption fine structure studies of polyoxometalate molecular cluster batteries: polyoxometalates as electron sponges, *J. Am. Chem. Soc.*, 2012, **134**, 4918–4924.
21 D. Pan, J. Chen, W. Tao, L. Nie and S. Yao, Phosphopolyoxomolybdate absorbed on lipid membranes/carbon nanotube electrode, *J. Electroanal. Chem.*, 2005, **579**, 77–82.
22 B. Fei, H. Lu, Z. Hu and J. H. Xin, Solubilization, purification and functionalization of carbon nanotubes using polyoxometalate, *Nanotechnology*, 2006, **17**, 1589–1593.
23 D. Pan, J. Chen, W. Tao, L. Nie and S. Yao, Polyoxometalate-modified carbon nanotubes: new catalyst support for methanol electro-oxidation, *Langmuir*, 2006, **22**, 5872–5876.
24 C. Warakulwit, J. Majimel, M. H. Delville, P. Garrigue, J. Limtrakul and A. Kuhn, Controlled purification,

solubilisation and cutting of carbon nanotubes using phosphomolybdic acid, *J. Mater. Chem.*, 2008, **18**, 4056–4061.

25 A. Giusti, G. Charron, S. Mazerat, J.-D. Compain, P. Mialane, A. Dolbecq, E. Rivière, W. Wernsdorfer, R. Ngo Biboum, B. Keita, L. Nadjo, A. Filoramo, J.-P. Bourgoin and T. Mallah, Magnetic bistability of individual single-molecule magnets grafted on single-wall carbon nanotubes, *Angew. Chem., Int. Ed.*, 2009, **48**, 4949–4952.

26 G. Charron, A. Giusti, S. Mazerat, P. Mialane, A. Gloter, F. Miserque, B. Keita, L. Nadjo, A. Filoramo, E. Riviere, W. Wernsdorfer, V. Huc, J. P. Bourgoin and T. Mallah, Assembly of a magnetic polyoxometalate on SWNTs, *Nanoscale*, 2010, **2**, 139–144.

27 J. Yuan, X. Jin, N. Li, J. Chen, J. Miao, Q. Zhang, L. Niu and J. Song, Large scale load of phosphotungstic acid on multi-walled carbon nanotubes with a grafted poly(4-vinylpyridine) linker, *Electrochim. Acta*, 2011, **56**, 10069–10076.

28 N. Kawasaki, H. Wang, R. Nakanishi, S. Hamanaka, R. Kitaura, H. Shinohara, T. Yokoyama, H. Yoshikawa and K. Awaga, Nanohybridization of polyoxometalate clusters and single-wall carbon nanotubes: applications in molecular cluster batteries., *Angew. Chem., Int. Ed.*, 2011, **123**, 3533–3536.

29 H. Wang, N. Kawasaki, T. Yokoyama, H. Yoshikawa and K. Awaga, Molecular cluster batteries of nano-hybrid materials between Keggin POMs and SWNTs, *Dalton Trans.*, 2012, **41**, 9863–9866.

30 M. Skunik, M. Chojak, I. A. Rutkowska and P. J. Kulesza, Improved capacitance characteristics during electrochemical charging of carbon nanotubes modified with polyoxometallate monolayers, *Electrochim. Acta*, 2008, **53**, 3862–3869.

31 M. Skunik and P. J. Kulesza, Phosphomolybdate-modified multi-walled carbon nanotubes as effective mediating systems for electrocatalytic reduction of bromate, *Anal. Chim. Acta*, 2009, **631**, 153–160.

32 A. K. Cuentas-Gallegos, R. Martínez-Rosales, M. Rincón, G. Hirata and G. Orozco, Design of hybrid materials based on carbon nanotubes and polyoxometalates, *Opt. Mater.*, 2006, **29**, 126–133.

33 F. M. Toma, A. Sartorel, M. Iurlo, M. Carraro, P. Parisse, C. Maccato, S. Rapino, B. R. Gonzalez, H. Amenitsch and T. Da Ros, Efficient water oxidation at carbon nanotube–polyoxometalate electrocatalytic interfaces, *Nat. Chem.*, 2010, **2**, 826–831.

34 Z. H. Kang, E. B. Wang, B. D. Mao, Z. M. Su, L. Gao, S. Y. Lian and L. Xu, Controllable fabrication of carbon nanotube and nanobelt with a polyoxometalate-assisted mild hydrothermal process, *J. Am. Chem. Soc.*, 2005, **127**, 6534–6535.

35 Z. Kang, Y. Wang, E. Wang, S. Lian, L. Gao, W. You, C. Hu and L. Xu, Polyoxometalates nanoparticles: synthesis, characterization and carbon nanotube modification, *Solid State Commun.*, 2004, **129**, 559–564.

36 W. Guan, Z. J. Wu and Z. M. Su, DFT study of ionic peapod structures from single-walled carbon nanotubes and Lindqvist tungstates, *Dalton Trans.*, 2012, **41**, 2798–2803.

37 E. Bichoutskaia, Z. Liu, N. Kuganathan, E. Faulques, K. Suenaga, I. J. Shannon and J. Sloan, High-precision imaging of an encapsulated Lindqvist ion and correlation of its structure and symmetry with quantum chemical calculations, *Nanoscale*, 2012, **4**, 1190–1199.

38 L. Hong, H. Tanaka and T. Ogawa, Rectification direction inversion in a phosphododecamolybdic acid/single-walled carbon nanotube junction, *J. Mater. Chem. C*, 2013, **1**, 1137–1143.

39 K. Suggs and X. Q. Wang, Structural and electronic properties of carbon nanotube-reinforced epoxy resins, *Nanoscale*, 2010, **2**, 385–388.

40 I. Ruiz-Tagle and W. Orellana, Iron porphyrin attached to single-walled carbon nanotubes: electronic and dynamical properties from *ab initio* calculations, *Phys. Rev. B: Condens. Matter Mater. Phys.*, 2010, **82**, 115406.

41 C. Sanchez, J. Livage, J. P. Launay, M. Fournier and Y. Jeannin, Electron delocalization in mixed-valence molybdenum polyanions, *J. Am. Chem. Soc.*, 1982, **104**, 3194–3202.

42 S. Z. Wen, W. Guan, J. P. Wang, Z. L. Lang, L. K. Yan and Z. M. Su, Theoretical investigation of structural and electronic properties of $[PW_{12}O_{40}]^{3-}$ on graphene layer, *Dalton Trans.*, 2012, **41**, 4602–4607.

43 P. Ordejón, E. Artacho and J. Soler, Self-consistent order-*N* density-functional calculations for very large systems, *Phys. Rev. B: Condens. Matter Mater. Phys.*, 1996, **53**, R10441–R10444.

44 D. Sánchez-Portal, P. Ordejón, E. Artacho and J. M. Soler, Density-functional method for very large systems with LCAO basis sets, *Int. J. Quantum Chem.*, 1997, **65**, 453–461.

45 J. M. Soler, E. Artacho, J. D. Gale, A. García, J. Junquera, P. Ordejón and D. Sánchez-Portal, The SIESTA method for *ab initio* order-*N* materials, *J. Phys.: Condens. Matter*, 2002, **14**, 2745–2779.

46 J. Junquera, Ó. Paz, D. Sánchez-Portal and E. Artacho, Numerical atomic orbitals for linear-scaling calculations, *Phys. Rev. B: Condens. Matter Mater. Phys.*, 2001, **64**, 235111.

47 T. Kostyrko, C. J. Lambert and B. R. Bułka, Current rectification in molecular junctions produced by local potential fields, *Phys. Rev. B: Condens. Matter Mater. Phys.*, 2010, **81**, 085308.

48 S. Z. Wen, G. C. Yang, L. K. Yan, H. B. Li and Z. M. Su, Theoretical study on rectifying performances of organoimido derivatives of hexamolybdates, *ChemPhysChem*, 2012, **14**, 610–617.

49 J. P. Perdew and A. Zunger, Self-interaction correction to density-functional approximations for many-electron systems, *Phys. Rev. B: Condens. Matter Mater. Phys.*, 1981, **23**, 5048–5079.

50 S. Z. Wen, W. Guan, Z. M. Su, L. K. Yan and S. Sanvito, First principle investigation transport properties of Lindqvist derivatives based molecular junction, *J. Mol. Graphics Modell.*, 2012, **38**, 220–225.

51 M. Dion, H. Rydberg, E. Schröder, D. C. Langreth and B. I. Lundqvist, Van der Waals density functional for general geometries, *Phys. Rev. Lett.*, 2004, **92**, 246401.

52 G. Román-Pérez and J. M. Soler, Efficient implementation of a van der Waals density functional: application to double-wall carbon nanotubes, *Phys. Rev. Lett.*, 2009, **103**, 096102.

53 J. P. Perdew, K. Burke and M. Ernzerhof, Generalized gradient approximation made simple, *Phys. Rev. Lett.*, 1996, **77**, 3865–3868.

54 R. S. Mulliken, Electronic population analysis on LCAO-MO molecular wave functions. I, *J. Chem. Phys.*, 1955, **23**, 1833.

55 A. Kokalj, Computer graphics and graphical user interfaces as tools in simulations of matter at the atomic scale, *Comput. Mater. Sci.*, 2003, **28**, 155–168.

56 X. López, J. M. Maestre, C. Bo and J. M. Poblet, Electronic properties of polyoxometalates: a DFT study of α/β-$[XM_{12}O_{40}]^{n-}$ relative stability (M = W, Mo and X a main group element), *J. Am. Chem. Soc.*, 2001, **123**, 9571–9576.

57 J. M. Maestre, X. López, C. Bo, J. M. Poblet and N. Casañ-Pastor, Electronic and magnetic properties of α-Keggin anions: a DFT study of $[XM_{12}O_{40}]^{n-}$, (M = W, Mo; X = $A1^{III}$, Si^{IV}, P^{V}, Fe^{III}, Co^{II}, Co^{III}) and $[SiM_{11}VO_{40}]^{m-}$ (M = Mo and W), *J. Am. Chem. Soc.*, 2001, **123**, 3749–3758.

58 J. M. Poblet, X. López and C. Bo, *Ab initio* and DFT modelling of complex materials: towards the understanding of electronic and magnetic properties of polyoxometalates, *Chem. Soc. Rev.*, 2003, **32**, 297–308.

59 X. Aparicio-Anglès, P. Miró, A. Clotet, C. Bo and J. M. Poblet, Polyoxometalates adsorbed on metallic surfaces: immediate reduction of $[SiW_{12}O_{40}]^{4-}$ on Ag(100), *Chem. Sci.*, 2012, **3**, 2020–2027.

60 X. Aparicio-Anglès, A. Clotet, C. Bo and J. M. Poblet, Towards the computational modelling of polyoxoanions on metal surfaces: IR spectrum characterisation of $[SiW_{12}O_{40}]^{4-}$ on Ag(111), *Phys. Chem. Chem. Phys.*, 2011, **13**, 15143–15147.

61 X. López, J. J. Carbó, C. Bo and J. M. Poblet, Structure, properties and reactivity of polyoxometalates: a theoretical perspective, *Chem. Soc. Rev.*, 2012, **41**, 7537–7571.

62 K. Seo, K. A. Park, C. Kim, S. Han, B. Kim and Y. H. Lee, Chirality-and diameter-dependent reactivity of NO_2 on carbon nanotube walls, *J. Am. Chem. Soc.*, 2005, **127**, 15724–15729.